Multioctave, 3–18 μm sub-two-cycle supercontinua from self-compressing, self-focusing soliton transients in a solid

A. A. Lanin,[1,2] A. A. Voronin,[1,2] E. A. Stepanov,[1,2] A. B. Fedotov,[1,2] and A. M. Zheltikov[1,2,3,*]

[1]Physics Department, International Laser Center, M. V. Lomonosov Moscow State University, Moscow 119992, Russia

[2]Russian Quantum Center, 143025 Skolkovo, Moscow Region, Russia

[3]Department of Physics and Astronomy, Texas A&M University, College Station, Texas 77843, USA

*Corresponding author: zheltikov@physics.msu.ru

Received December 8, 2014; accepted January 5, 2015;
posted January 14, 2015 (Doc. ID 229271); published March 10, 2015

Strongly coupled nonlinear spatiotemporal dynamics of ultrashort mid-infrared pulses undergoing self-focusing simultaneously with soliton self-compression in an anomalously dispersive, highly nonlinear solid semiconductor is shown to enable the generation of multioctave supercontinua with spectra spanning the entire mid-infrared range and compressible to subcycle pulse widths. With 7.9 μm, 150 fs, 2 μJ, 1 kHz pulses used as a driver, 1.2 cycle pulses of mid-infrared supercontinuum radiation with a spectrum spanning the range of wavelengths from 3 to 18 μm were generated in a 5 mm GaAs plate. Further compression of these pulses to subcycle pulse widths is possible through compensation of the residual phase shift. © 2015 Optical Society of America

OCIS codes: (320.5520) Pulse compression; (320.7110) Ultrafast nonlinear optics.
http://dx.doi.org/10.1364/OL.40.000974

Ultrafast optics in the mid-infrared (mid-IR) is a rapidly growing field of research, gaining a new momentum from the development of high-power sources of ultrashort mid-infrared pulses [1] and novel methods of broadband field waveform characterization in the mid-infrared [2,3]. The cutting-edge technologies for mid-IR pulse generation [1], which have been recently extended to the subterawatt level of peak powers [4], offer new approaches for coherent [5] and incoherent [6] x-ray generation, open the routes toward subattosecond pulse generation [5], enable mid-IR laser filamentation in the atmosphere [4], help achieve lasing in filaments [7], give rise to unique regimes of laser-matter interactions [8], and reveal unexpected properties of materials in the mid-IR range [9].

In view of this impressive progress, the key question to be addressed is to what extent the nonlinear-optical strategies of pulse compression and coherent broadband waveform generation can be extended to the mid-IR range. In the near-infrared, the physical scenarios behind these processes have been thoroughly understood, enabling highly efficient technologies for few- and even single-cycle pulse generation, as well as efficient supercontinuum generation for a vast variety of applications, ranging from optical parametric amplification of ultrashort pulses to spectroscopy and bioimaging. The extension of these scenarios to the mid-IR is, however, in no way trivial. The main difficulties include a nonuniform, often complex wavelength scaling of the key ultrafast nonlinear phenomena and optical nonlinearities of materials. Fiber-optic strategies, which play the key role in ultrafast nonlinear optics in the near-infrared [10] and which offer much promise for mid-IR photonics [11,12], are not easily scalable to higher peak powers. As a result, nonlinear-optical transformation of ultrashort mid-IR pulses in bulk solids attracts much interest [13–18] as a realistic option for pulse compression and supercontinuum generation of mid-IR pulses with moderate peak powers.

Much experimental effort has been made to identify promising regimes of pulse compression and supercontinuum generation in this scheme beyond the standard Ti:sapphire range [13,14]. However, only a few experiments have been performed so far with driver wavelengths longer than 3 μm, that is, in the most interesting and most challenging region of the mid-IR range. As a part of that effort, following the seminal work by Corkum *et al.* [13], Ashihara and Kawahara [15] demonstrated a spectral broadening of 100 fs, 2.8 μJ pulses at a central wavelength of 5 μm in GaAs, yielding supercontinuum radiation with a spectrum stretching from 3.6 to 6.4 μm. Silva *et al.* [16] used 80 fs, 6.9 μJ pulses at a central wavelength of 3.1 μm to generate a supercontinuum with a spectrum stretching from 450 nm to 4.5 μm if measured at the 40 dB level. Hemmer *et al.* [17] have demonstrated that such supercontinua are compressible to sub-three-cycle pulse widths. At a radically different level of field intensities, experiments with millijoule 80 fs pulses with a central wavelength of 3.9 μm and a peak power orders of magnitude higher than the self-focusing threshold have revealed [18] filamentation-assisted self-compression to a pulse width of 40 fs accompanied by the generation of ultrabroadband supercontinuum radiation. Finally, generation of tunable few-cycle pulses in the wavelength range from 4.2 to 6.8 μm was demonstrated [3] with the use of self-focusing-assisted spectral broadening in a normally dispersive, highly nonlinear semiconductor material, followed by pulse compression in the regime of anomalous dispersion.

In this work, we move further on into the mid-IR, toward longer driver wavelengths, and explore the potential of anomalously dispersive nonlinear materials for pulse self-compression and supercontinuum generation in the mid-IR. Soliton-based self-compression of optical field waveforms in the regime of anomalous dispersion has long been recognized [10] as an

interesting alternative to a standard pulse compression technique based on spectral broadening in a normal-dispersion medium followed by chirp compensation in an anomalously dispersive material. In the mid-IR range, soliton-based scenarios of self-compression are of special significance since many highly nonlinear materials possess anomalous dispersion in this spectral region.

In experiments, we use a frequency-tunable source of ultrashort pulses in the mid-IR [3], which involves two sequential stages of nonlinear-optical down conversion (Fig. 1). At the first stage, 65 fs, 0.8 mJ, 810 nm, 1 kHz pulses delivered by a Ti:sapphire laser, consisting of a master oscillator and a multipass amplifier, are used to produce a broadband seed signal through supercontinuum generation in a sapphire plate and serve as a pump for optical parametric amplification (OPA) of the seed signal in a BBO crystal, yielding signal and idler fields tunable in the 1150–1580 nm and 1620–2300 nm ranges, respectively. At the second stage, the signal and idler OPA outputs are used to produce a wavelength-tunable field in the mid-IR (Fig. 1) through difference-frequency generation (DFG) in an $AgGaS_2$ (AGS) crystal [19]. The central wavelength of the DFG signal generated as a result of this process can be tuned from 2.85 to 13 μm by rotating the AGS crystal.

The signal and idler pulses delivered by the OPA are characterized using cross-correlation frequency-resolved optical gating (XFROG) by sum-frequency-mixing these pulses with the 65 fs, 810 nm Ti:sapphire laser output in a thin, 50 μm BBO crystal. The spectrum of the DFG radiation is measured with the use of a pyroelectric or cooled HgCdTe detector connected with a lock-in amplifier and a homemade monochromator, with replaceable 75, 150, and 300 grooves/mm gratings.

Mid-IR pulses are characterized in our experiments using the XFROG technique based on four-wave mixing (FWM) in a gas medium [2,3]. To this end, an ultrashort mid-IR pulse is combined with a reference Ti:sapphire laser pulse on an off-axis 100 mm focal length parabolic mirror with a hole, which focuses both pulses into a molecular or atomic gas (Fig. 1) to generate an FWM signal through the $\omega_{FWM} = 2\omega_p - \omega_d$ process. The FWM signal is then collimated with a 75 mm focal length BK7 glass lens, separated from the infrared beams with a set of appropriate filters, and analyzed using an Ocean Optics spectrometer.

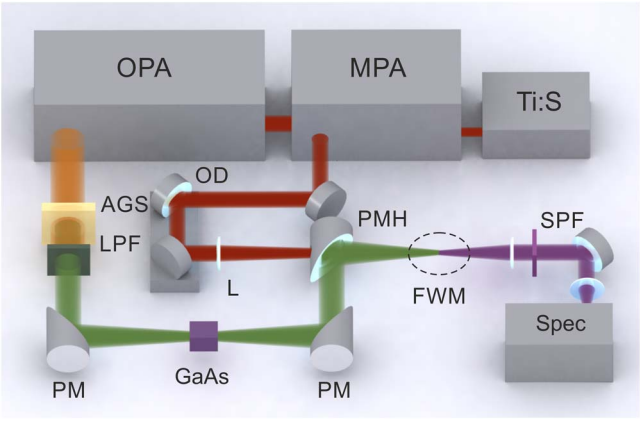

Fig. 1. Experimental setup. Ti:S, mode-locked Ti:sapphire master oscillator; MPA, multipass amplifier; OPA, optical parametric amplifier; AGS, $AgGaS_2$ crystal; LPF, longpass filter; PM, parabolic mirror; L, BK7 glass lens; OD, optical delay line; PMH, parabolic mirror with a hole; FWM, four-wave mixing in a gas medium; SPF, shortpass filter; Spec, spectrometer.

Soliton self-compression of the wavelength-tunable mid-IR DFG output is implemented in our experiments using GaAs, which possesses a high nonlinearity, $n_2 \approx 3 \cdot 10^{-14}$ cm^2/W, and an anomalous dispersion for wavelengths longer than its zero group-velocity-dispersion wavelength, $\lambda_z \approx 6.8$ μm. The 150 fs, 1–3 μJ DFG output with a central wavelength tunable from 7.1 to 8.5 μm is focused in our experiments with a 75 mm focal length off-axis parabolic mirror and transmitted through a 5 mm thick GaAs plate (Fig. 1). Nonlinear transformation of mid-IR pulses in GaAs gives rise to supercontinuum radiation, whose spectrum may in certain regimes span more than two octaves in the mid-IR range [Figs. 2(a)–2(e)]. With a DFG output with an initial pulse width $\tau_0 \approx 150$ fs, central wavelength $\lambda_0 \approx 7.9$ μm, and input energy $W_0 \approx 2$ μJ used as a driver, supercontinuum generation in a 5 mm GaAs plate yields a spectrum spanning the range of wavelengths from 3 to 18 μm [Fig. 2(e)].

Supercontinuum generation is accompanied by pulse self-compression. Temporal envelopes of the supercontinuum output retrieved from the FWM XFROG traces show that pulse compression ratios exceeding 3 are

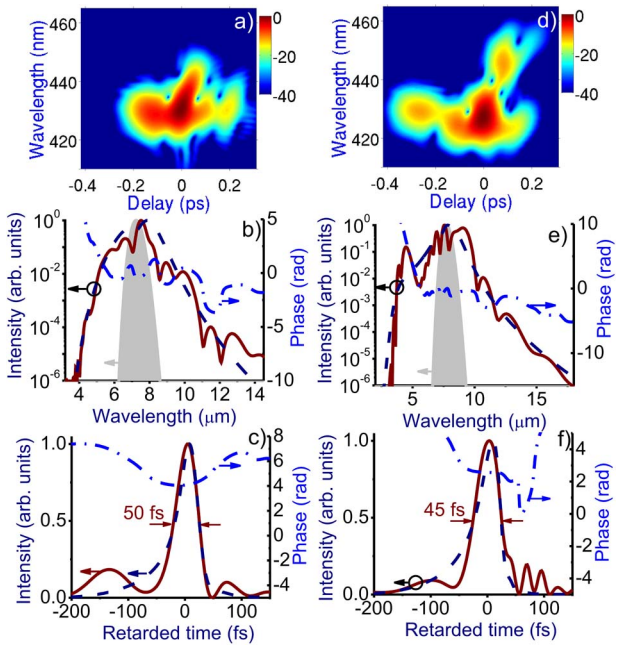

Fig. 2. Self-compression of mid-IR pulses with an initial pulse width $\tau_0 \approx 150$ fs, central wavelength (a)–(c) $\lambda_0 \approx 7.1$ μm and (d)–(f) 7.9 μm, and input energy $W_0 \approx 2$ μJ in a 5-mm GaAs plate. (a), (d) An FWM XFROG trace of the mid-IR pulse behind the GaAs plate. (b), (e) The input spectrum of the pulse (gray shading), experimental (solid line) and simulated (dashed line) output spectra, and the spectral phase (dashed–dotted line) of the output waveform retrieved from the FWM XFROG trace. (c), (f) Experimental (solid line) and simulated (dashed line) temporal envelope of the mid-IR pulse behind the GaAs plate with the phase (dashed–dotted line) retrieved from the FWM XFROG trace.

achieved within a broad range of wavelengths [Figs. 2(c) and 2(f)], stretching at least from 7.1 to 8.4 μm. Specifically, a mid-IR DFG output with $\tau_0 \approx 150$ fs, $\lambda_0 \approx 7.9$ μm, and $W_0 \approx 2$ μJ undergoes spectral broadening and self-compression in a 5 mm GaAs plate, evolving to a waveform with a pulse width $\tau_c \approx 45$ fs behind this plate [Fig. 2(f)]. Such a pulse contains only 1.2 cycles of the field at $\lambda_0 \approx 7.9$ μm.

To understand the spatiotemporal dynamics of ultrashort pulses behind the generation of sub-two-cycle field waveforms in the mid-IR in a highly nonlinear, anomalously dispersive material, we performed numerical modeling using the three-dimensional time-dependent generalized nonlinear Schrödinger equation (GNSE) [20,21] for the amplitude of the field, including all the key physical phenomena, such as dispersion, beam diffraction, Kerr nonlinearity, pulse self-steepening, spatial self-action phenomena, ionization-induced optical nonlinearities, as well as plasma loss and dispersion. The field evolution equation is solved jointly with the rate equation for the electron density, which includes photoionization and impact ionization. Simulations are performed for typical parameters of GaAs—a band gap of 1.4 eV, the Kerr-effect nonlinear refractive index $n_2 \equiv n_{\mathrm{GaAs}} \approx 3 \cdot 10^{-14}$ cm^2/W, and the higher order Kerr effect (HOKE) coefficient $n_4 \approx 2 \cdot 10^{-26}$ cm^4/W^2 [22]. Dispersion of GaAs was included in the model through the Sellmeier equation [23]. Simulations were performed using an MPI parallel programming interface on the Chebyshev and Lomonosov supercomputer clusters of Moscow State University.

Numerical simulations reproduce all the key features and tendencies in supercontinuum spectra [Figs. 2(b) and 2(e)] and pulse shapes [Figs. 2(c) and 2(f)], demonstrating the predictive power of our model. To fully realize the advantages offered by the anomalous dispersion regime for pulse compression in the mid-IR, it is instructive to artificially decouple the temporal field evolution from spatial beam dynamics and compare pulse self-compression dynamics in a standard soliton, defined as the solution to the nonlinear Schrödinger equation (NSE) [10], with the evolution of an ultrashort pulse with the same parameters, $\tau_0 \approx 150$ fs, $\lambda_0 \approx 7.9$ μm, and $W_0 \approx 2$ μJ, in a hypothetical medium with the same nonlinearity, but normal dispersion. The NSE models neglect higher order dispersion and HOKE effects, describing the nonlinearity and dispersion of a medium in terms of the nonlinear coefficient n_2 and group-velocity dispersion coefficient β_2. For NSE-soliton simulations, we take $\beta_2 \equiv \beta_{\mathrm{GaAs}} \approx 0.2$ ps^2/m, as dictated by the Sellmeier equation for GaAs at $\lambda_0 \approx 7.9$ μm. For a fair comparison, calculations for pulse evolution in the normal dispersion regime are performed with $\beta_2 = |\beta_{\mathrm{GaAs}}|$. For the chosen set of parameters, we then find that the dispersion length is $l_d = 4$ cm and the nonlinear length is $l_{\mathrm{nl}} \approx 1.8$ mm, giving the soliton number $N = (l_d/l_{\mathrm{nl}})^{1/2} \approx 4.7$.

In the regime of normal dispersion [Figs. 3(a) and 3(b)], the spectral broadening of an ultrashort pulse due to self-phase modulation is limited by dispersion-induced pulse stretching, increasing the pulse width up to 210 fs at $z = 5$ mm [Fig. 3(b)]. In the regime of anomalous dispersion, the NSE-model pulse dynamics is strikingly different [Figs. 3(c) and 3(d)]. With pulse

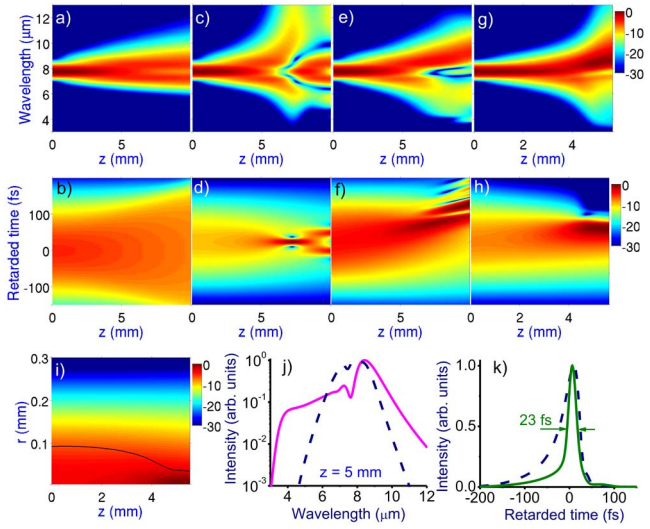

Fig. 3. (a)–(h) The spectral [(a), (c), (e), (g)] and temporal [(b), (d), (f), (h)] evolution of ultrashort mid-IR pulses $\lambda_0 \approx 150$ fs, $\lambda_0 \approx 7.9$ μm, and $W_0 \approx 2$ μJ (a), (b) in a medium with normal dispersion with $\beta_2 = |\beta_{\mathrm{GaAs}}|$ and $n_2 = n_{\mathrm{GaAs}}$, (c), (d) in an ideal NSE soliton in GaAs, (e), (f) in GaAs without spatial self-action effects, and (g), (h) in GaAs with high-order dispersion, self-steepening, and spatial self-action effects included. (i) The beam dynamics in the mid-IR pulse propagating through GaAs. The FWHM beam radius is shown by the black line. (j) The spectrum of the mid-IR pulse at $z = 5$ mm with (solid line) and without (dashed line) spatial self-action effects included in the model. (k) Simulated temporal envelopes of the mid-IR pulse behind the GaAs plate (dashed line) and following additional chirp compensation in a BaF_2 plate with a thickness of 350 μm.

stretching suppressed due to anomalous dispersion and with $N \gg 1$ for the chosen parameters, the bandwidth of the pulse grows exponentially at the initial stage of pulse evolution, i.e., for $z \ll l_d$ [Fig. 3(c)]. At later stages, dispersion catches up, compressing the pulse [Fig. 3(d)] to a pulse width $\tau_s \approx 0.24\tau_0/(N-1)$ [12]. For the chosen parameters, the on-axis field intensity at $z = 5$ mm in the regime of anomalous dispersion (0.22 TW/cm^2) is almost an order of magnitude higher than the on-axis field intensity at the same point in the normal dispersion regime.

The textbook scenario of soliton self-compression outlined above can be modified [20,21] by high-order dispersion, self-steepening, ionization, and spatial self-action effects. Our simulations show that, for the chosen range of field intensities, the electron density induced in GaAs by the mid-IR driver rapidly grows toward the exit surface of the GaAs plate, but remains well below 10^{16} cm^{-3} for $z < 4$ mm, reaching the level of 10^{17} cm^{-3} only at $z = 5$ mm. At this level of electron densities, ionization effects have virtually no influence on soliton dynamics.

Self-steepening, which becomes significant as the bandwidth of the mid-IR pulse becomes larger than an octave as a result of spectral broadening, enhances the short-wavelength wing of the spectrum and partially suppresses its long-wavelength tail [Fig. 3(e)]. High-order dispersion removes the group-velocity degeneracy, inducing a fission of high-N solitons [10], arising as a part

of the soliton dynamics considered here. The fissioning solitons are clearly seen for $z > 5$ mm in Fig. 3(f).

Spatial self-action is of key significance for soliton self-compression in our experiments. In the considered range of peak powers, self-focusing suppresses diffraction-induced beam divergence. The beam dynamics in the mid-IR driver is illustrated in Fig. 3(i), where the black line presents the FWHM beam radius, visualizing the self-focusing of the mid-IR beam. The characteristic focusing length of the Kerr-effect-induced nonlinear lens, $l_{sf} \approx 5.3$ mm, is very close to the thickness of the GaAs plate. Such a nonlinear lens, whose focal length is matched with the nonlinear interaction length, keeps the field intensity high, thus helping to maintain the soliton dynamics along the entire propagation path within the GaAs plate despite diffraction [Fig. 3(h)]. As a result, the spectrum of the mid-IR supercontinuum at the exit interface of the GaAs plate, $z = 5$ mm in Figs. 3(g) and 3(h), has a spectrum stretching from 3 to 18 μm [Fig. 2(e) and solid line in Fig. 3(j)], with its pulse width, $\tau_c \approx 45$ fs, corresponding to only 1.2 cycles of the field at $\lambda_0 \approx 7.9$ μm. Moreover, with an additional chirp compensation in a thin plate of anomalously dispersive material (a 350 μm thick BaF_2 plate), this self-compressed supercontinuum output can be further compressed, as our simulations show, to a subcycle pulse width of 23 fs [Fig. 3(k)]. For comparison, the dashed line in Fig. 3(j) presents the spectrum of supercontinuum produced under the same conditions, but with the self-focusing term of the GNSE disabled in simulations. This spectrum is seen to be much narrower because of a considerable decrease in the field intensity toward the exit surface of the nonlinear medium induced by diffraction.

To summarize, we have shown in this work that a strongly coupled nonlinear spatiotemporal dynamics of ultrashort mid-IR pulses undergoing self-focusing simultaneously with soliton self-compression in an anomalously dispersive, highly nonlinear solid semiconductor can provide a source of multioctave supercontinua with spectra spanning the entire mid-IR range and compressible to subcycle pulse widths. With 7.9 μm, 150 fs, 2 μJ, 1 kHz pulses used as a driver, 1.2 cycle pulses of mid-IR supercontinuum with a spectrum stretching from 3 to 18 μm were generated in a 5 mm GaAs plate. A further compression of these pulses to subcycle pulse widths is possible through a straightforward compensation of the residual phase shift.

This research was supported in part by the Russian Foundation for Basic Research (project nos. 13-02-01465, 13-02-92115, 14-02-00784, 14-22-02099, and 15-02-07820) and the Welch Foundation (grant no. A-1801). Research into the nonlinear optics in the mid-infrared has been supported by the Russian Science Foundation (project no. 14-12-00772).

References

1. G. Andriukaitis, T. Balčiūnas, S. Ališauskas, A. Pugžlys, A. Baltuška, T. Popmintchev, M.-C. Chen, M. M. Murnane, and H. C. Kapteyn, Opt. Lett. **36**, 2755 (2011).
2. Y. Nomura, H. Shirai, K. Ishii, N. Tsurumachi, A. A. Voronin, A. M. Zheltikov, and T. Fuji, Opt. Express **20**, 24741 (2012).
3. A. A. Lanin, A. A. Voronin, E. A. Stepanov, A. B. Fedotov, and A. M. Zheltikov, Opt. Lett. **39**, 6430 (2014).
4. A. V. Mitrofanov, A. A. Voronin, D. A. Sidorov-Biryukov, A. Pugžlys, E. A. Stepanov, G. Andriukaitis, T. Flöry, S. Ališauskas, A. B. Fedotov, A. Baltuška, and A. M. Zheltikov, http://arXiv.org/abs/1410.2647.
5. T. Popmintchev, M.-C. Chen, D. Popmintchev, P. Arpin, S. Brown, S. Alisauskas, G. Andriukaitis, T. Balciunas, O. D. Mücke, A. Pugzlys, A. Baltuska, B. Shim, S. E. Schrauth, A. Gaeta, C. Hernandez-Garcia, L. Plaja, A. Becker, A. Jaron-Becker, M. M. Murnane, and H. C. Kapteyn, Science **336**, 1287 (2012).
6. J. Weisshaupt, V. Juvé, M. Holtz, S. Ku, M. Woerner, T. Elsaesser, S. Ališauskas, A. Pugžlys, and A. Baltuška, Nat. Photonics **8**, 927 (2014).
7. D. Kartashov, S. Ališauskas, G. Andriukaitis, A. Pugžlys, M. Shneider, A. Zheltikov, S. L. Chin, and A. Baltuška, Phys. Rev. A **86**, 033831 (2012).
8. E. E. Serebryannikov and A. M. Zheltikov, Phys. Rev. Lett. **113**, 043901 (2014).
9. D. Kartashov, S. Ališauskas, A. Pugžlys, A. A. Voronin, A. M. Zheltikov, and A. Baltuška, Opt. Lett. **37**, 2268 (2012).
10. G. P. Agrawal, *Nonlinear Fiber Optics* (Academic, 2001).
11. C. R. Petersen, U. Møller, I. Kubat, B. Zhou, S. Dupont, J. Ramsay, T. Benson, S. Sujecki, N. Abdel-Moneim, Z. Tang, D. Furniss, A. Seddon, and O. Bang, Nat. Photonics **8**, 830 (2014).
12. Y. Yu, X. Gai, T. Wang, P. Ma, R. Wang, Y. Zhiyong, D.-Y. Choi, S. Madden, and B. Luther-Davies, Opt. Mater. Express **3**, 1075 (2013).
13. P. B. Corkum, P. P. Ho, R. R. Alfano, and J. T. Manassah, Opt. Lett. **10**, 624 (1985).
14. M. Durand, A. Jarnac, A. Houard, Y. Liu, S. Grabielle, N. Forget, A. Durécu, A. Couairon, and A. Mysyrowicz, Phys. Rev. Lett. **110**, 115003 (2013).
15. S. Ashihara and Y. Kawahara, Opt. Lett. **34**, 3839 (2009).
16. F. Silva, D. R. Austin, A. Thai, M. Baudisch, M. Hemmer, D. Faccio, A. Couairon, and J. Biegert, Nat. Commun. **3**, 807 (2012).
17. M. Hemmer, M. Baudisch, A. Thai, A. Couairon, and J. Biegert, Opt. Express **21**, 28095 (2013).
18. A. Pugzlys, P. Malevich, S. Alisauskas, A. A. Voronin, D. Kartashov, A. Baltuska, A. Zheltikov, and D. Faccio, *Technical Digest of Conference on Lasers and Electro-Optics* (Optical Society of America, 2014), paper FTh1D.3.
19. R. A. Kaindl, M. Wurm, K. Reimann, P. Hamm, A. M. Weiner, and M. Woerner, J. Opt. Soc. Am. B **17**, 2086 (2000).
20. L. Bergé, S. Skupin, R. Nuter, J. Kasparian, and J.-P. Wolf, Rep. Prog. Phys. **70**, 1633 (2007).
21. A. A. Voronin and A. M. Zheltikov, Phys. Rev. A **90**, 043807 (2014).
22. D. Milam, M. J. Weber, and A. J. Glass, Appl. Phys. Lett. **31**, 822 (1977).
23. M. Bass, C. DeCusatis, J. Enoch, V. Lakshminarayanan, G. Li, C. MacDonald, V. Mahajan, and E. Van Stryland, *Handbook of Optics*, 3rd ed. (McGraw-Hill, 2009), Vol. **4**.